Ore Geology Reviews 84 (2017) 102–115

Contents lists available at ScienceDirect

Ore Geology Reviews

journal homepage: www.elsevier.com/locate/oregeo

# Uranyl phosphates and associated minerals in the Koprubasi (Manisa) uranium deposit, Turkey

Hulya Kacmaz [a,*], Peter C. Burns [b]

[a] Dokuz Eylul University, Faculty of Engineering, Department of Geological Engineering, Tinaztepe-Buca-35160, Izmir, Turkey
[b] University of Notre Dame, Department of Civil & Environmental Engineering & Earth Sciences, Department of Chemistry and Biochemistry, Notre Dame, IN, USA

ARTICLE INFO

*Article history:*
Received 29 September 2015
Received in revised form 21 October 2016
Accepted 2 January 2017
Available online 4 January 2017

*Keywords:*
Uranium
Autunite
Torbernite
Fe-(hydr) oxide
Clay

ABSTRACT

The Koprubasi uranium deposit is the largest known uranium deposits in Turkey. Uranium mineralization is hosted in Neogene fluvial sediments that consist of predominantly sandstone and conglomerate interlayered with siltstone, claystone and mudstone. Sediments were primarily derived from metamorphic rocks adjacent to the basins of deposition, with some volcanic contribution in the form of tuffs. The sandstones and conglomerates are the most widespread sediments within the study area and host the majority of the U ore.

X-ray diffraction (XRD) and scanning electron microscopy (SEM) with energy-dispersive X-ray spectroscopy (EDX) analysis were used to identify the ore and associated minerals. The uranium ore minerals of the host sedimentary rocks are torbernite, meta-torbernite and meta-autunite. These coexist with jarosite, various clays (chlorite/kaolinite, illite, and smectite), and Fe- and Mn-(hydr) oxides with minor titanium oxide. Additionally, quartz, feldspars and a minor amount of mica (muscovite and biotite) are the main primary minerals in the sedimentary rocks.

The uranyl phosphates coat the surfaces of pebbles and some mineral grains, fill cracks, and are disseminated within the pores of the host sedimentary rocks. Uranyl phosphates are commonly associated with Fe-(hydr) oxides and clays, although some were observed in millimeter- or centimeter wide gaps within Koprubasi sediments. Oxides of manganese are also locally abundant and associated with uranyl phosphates.

The uranyl phosphates in the sediments of the Koprubasi area most likely formed when oxidizing groundwater moved through the host rock. The common association of uranyl phosphates with Fe-(hydr) oxides and clays suggests that the precipitation of uranyl phosphate minerals is mainly due to adsorption of the uranyl and phosphate to the surface of Fe-(hydr) oxides and clays.



## 1. Introduction

Koprubasi is located 120 km northeast of Manisa in western Turkey (Fig. 1). It has a typical Mediterranean climate with hot and dry summers, and mild and rainy winters. Uranium exploration in the Koprubasi area commenced in 1957 under the General Directorate of Mineral Research and Exploration of Turkey (MTA), which led to discovery of the Koprubasi uranium deposit in 1961 (Manisa) as a result of aerial and ground surveys.

Since the discovery of the Koprubasi uranium deposit, limited studies have been conducted to evaluate the geology, mineralogy, origin, and reserves of uranium (Maden Tetkik Arama, 1976; Yılmaz, 1982). Although the presence of some uranyl minerals is suggested by Maden Tetkik Arama (1976), there has been no characterization of the uranium and associated minerals and their relationships. Also, the coexistence of uranium minerals with Fe-and Mn-(hydr) oxides, clays and titanium oxides has not been previously recognized in the Koprubasi uranium deposit.

The aim of our study is to characterize the mineralogy of the Koprubasi (Manisa) uranium deposit and to examine the effect of Fe-(hydr) oxides and clays on the precipitation of uranyl phosphates. To our knowledge, this study is the first investigation reporting uranium phosphate minerals associated with Fe-(hydr) oxides (like goethite) and clays in this deposit.

## 2. Geological setting

Koprubasi is a district within the Manisa Province in the Aegean region of Turkey. The lithological units exposed at Koprubasi

* Corresponding author.
*E-mail address:* hulya.kacmaz@deu.edu.tr (H. Kacmaz).

http://dx.doi.org/10.1016/j.oregeorev.2017.01.001
0169-1368/

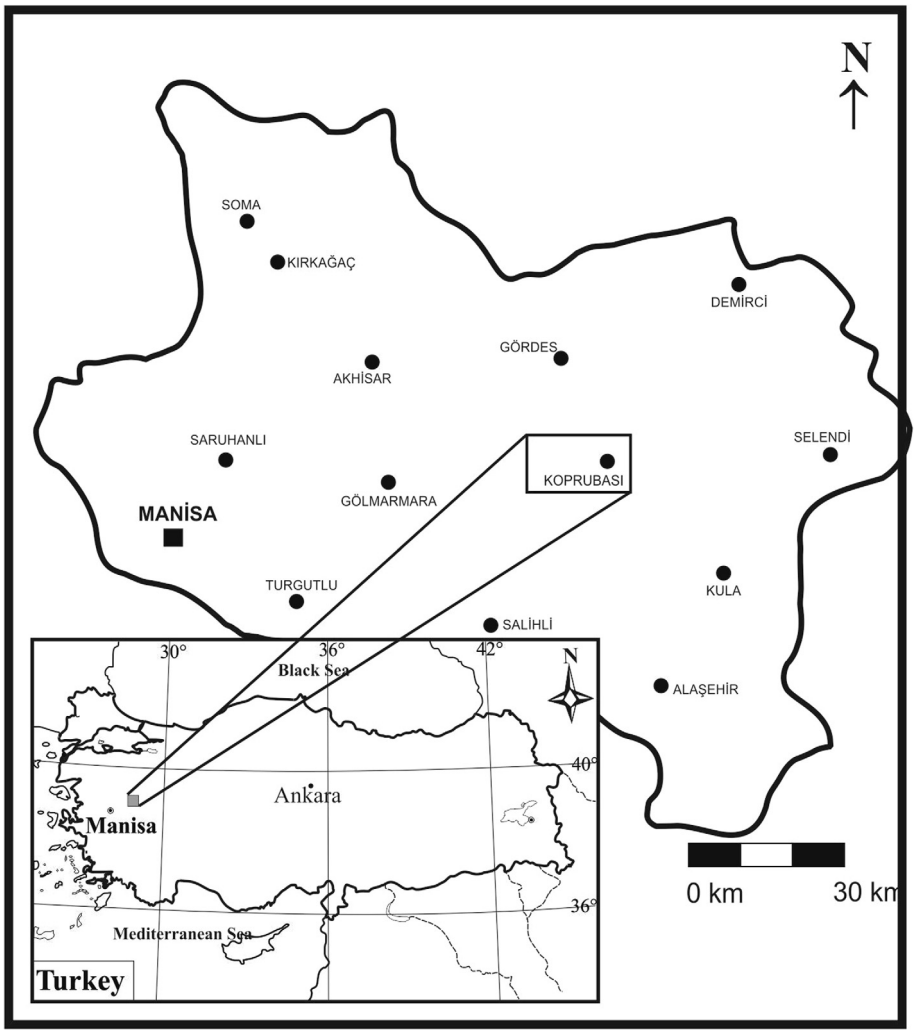


**Fig. 1.** Location map of the study area.

(Manisa) and nearby consist of metamorphic and sedimentary rocks. The basement metamorphic rocks are mainly banded and biotite gneisses belonging to Menderes Massif. The banded gneiss contains pegmatite dykes and quartz veins. The metamorphic rocks are overlain unconformably by Neogene sedimentary rocks consisting of, from bottom to top, fluvial and lacustrine sedimentary rocks. Neogene fluvial sedimentary rocks consist predominantly of sandstone and conglomerate interlayered with siltstone, claystone and mudstone. They are also interbedded with acidic tuffs and silicified stratum in some areas. Neogene fluvial sedimentary rocks are overlain by lacustrine sedimentary rocks that cover a small portion of the southern part of the study area that is well exposed at Tulluce. These combine mudstone, marl, siltstone and limestones, and the contact between lacustrine and fluvial sedimentary rocks is gradational (Maden Tetkik Arama, 1976; Yılmaz, 1982).

## 3. Samples and analytical techniques

Uranium mineralization occurs in various localities around the Koprubasi area (Maden Tetkik Arama, 1976). Therefore, radiometric measurements with a geiger counter was done while travelling by foot, principally around the Koprubasi area. The strongest radioactivities were detected at the Kasar, Ecinlitas, Topalli, Cetinbas, Ugurlu and Kayran areas. Hence, this study is focused on these areas (Fig. 2).

All samples were collected from outcrops. A portion of each sample was crushed and pulverized for subsequent chemical analyses, and a piece of each sample was retained for detailed mineralogical and petrologic studies. The textures of some sediment samples were examined in polished thin sections and in polished epoxy mounts. The mineralogy of sediment samples was determined by powder X-ray diffraction (XRD) using a Rigaku D/Max-2200 Ultima$^{+}$/PC diffractometer (at the Turkish Petroleum Corporation in Turkey) and a Bruker Davinci diffractometer (at the University of Notre Dame in the USA). Diffraction data were collected from randomly oriented powders. The powder specimen was packed into the cavity of the glass sample holder and then its surface was smoothed with another glass slide. The scans were conducted from 2 to 70° at 0.02°2θ step size and 1 s per step data collection time using Cu $K\alpha$ X-radiation. Additionally, where weak reflections were observed using the previously stated scan rate, additional scans were collected at 10 s per step to increase the signal to noise ratio.

A JEOL-JSM 6060 (at Dokuz Eylul University in Turkey) and EVO 50 LEO SEM and FEI-MAGELLAN 400 FESEM (at University of Notre Dame in the USA) scanning electron microscope (SEM) equipped with an energy-dispersive X-ray spectrometer (EDX) were used to characterize uranium and associated mineral morphologies. Samples for SEM-EDX analysis were prepared by adhering sediment samples with freshly broken surfaces onto an aluminum stub with double-sided carbon tape, with each sample also coated with

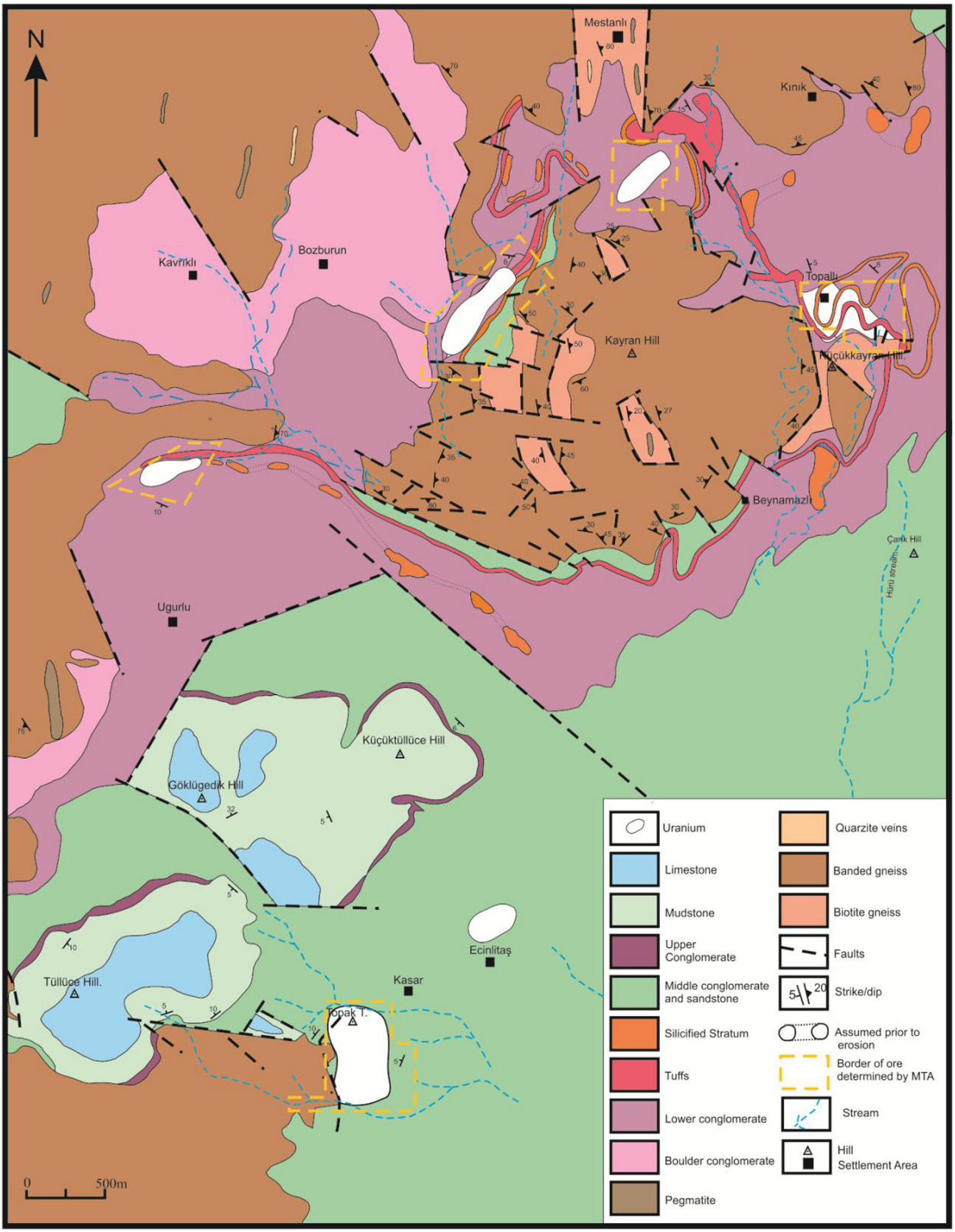


**Fig. 2.** Geological map of the study area (modified from Maden Tetkik Arama, 1976 and Yılmaz, 1982) showing uranium mineralization.

Au. Backscattered-electron imaging (BSE) and elemental mapping using the SEM were also applied to the samples.

## 4. Host rock

The uranium deposits occur in Neogene fluvial sedimentary rocks that unconformably overlie basement metamorphic rocks. The primary source of these sediments is banded and biotite gneisses. Gneiss composed mostly of mica (biotite and muscovite), feldspar, quartz, chlorite/kaolinite and illite with a lesser amount of jarosite. Apatite, zircon, ilmenite, pyrite, titanite and rutile are also present as accessory minerals. Apatite is a common accessory mineral and is generally associated with and surrounded by biotite.

The sandstones and conglomerates are the most widespread sedimentary rocks within the study area and host the majority of the U ore minerals. The colors of sandstone and conglomerate are quite variable. They are generally yellowish brown, reddish brown or greenish grey with lesser brown-black colors. The greenish grey sandstones contain higher amounts of mica and clay. However, pale yellow areas occur in some greenish grey sandstone that are the product of $Fe^{2+}$-bearing sulfide oxidation.

The chief mineralogical constituents of the sandstone and conglomerate are quartz, feldspar, micas (biotite and muscovite), clays, Fe-(hydr) oxides and metamorphic rock fragments. The rock fragments consist mainly of gneiss with lesser tuff. They are cemented by iron oxides and silica or clays. Quartz is the most abundant detrital mineral in the sandstone and conglomerate. The detrital grains are angular to subangular in shape. Size sorting of the detrital grain is generally poor, indicating rapid deposition. Most of the muscovite grains are fresh, only rarely altered to illite. Biotite is partly or completely altered to chlorite. Feldspar is partly altered to illite, kaolinite and smectite. The ferric sulfate mineral jarosite ($KFe_3(SO_4)_2(OH)_6$) occurs in pale yellow patches in some sandstone.

The XRD studies show that the most abundant minerals in the uranium-hosted sandstone and conglomerate are quartz, feldspar, chlorite/kaolinite, jarosite, mica (muscovite/biotite/illite) and smectite (Fig. 3). On the other hand, no significant differences were found between the sandstone and conglomerate mineralogy.

## 5. Results and discussion

### 5.1. Uranyl phosphates

The majority of the U-mineralization in the Koprubasi sediments occurs within the sandstones and conglomerates interlayered with mudstone, claystone, and siltstone. Macroscopic uranium minerals can be easily located as they are faint green and greenish-yellow grains within the conglomerate and sandstone. In these, the U minerals generally coat the surfaces of individual silicate grains, filling cracks and voids. In addition, microscopic U ore minerals can be identified by using ultraviolet light, and are disseminated in the pores of the conglomerate and sandstone. Torbernite, meta-torbernite and meta-autunite are the

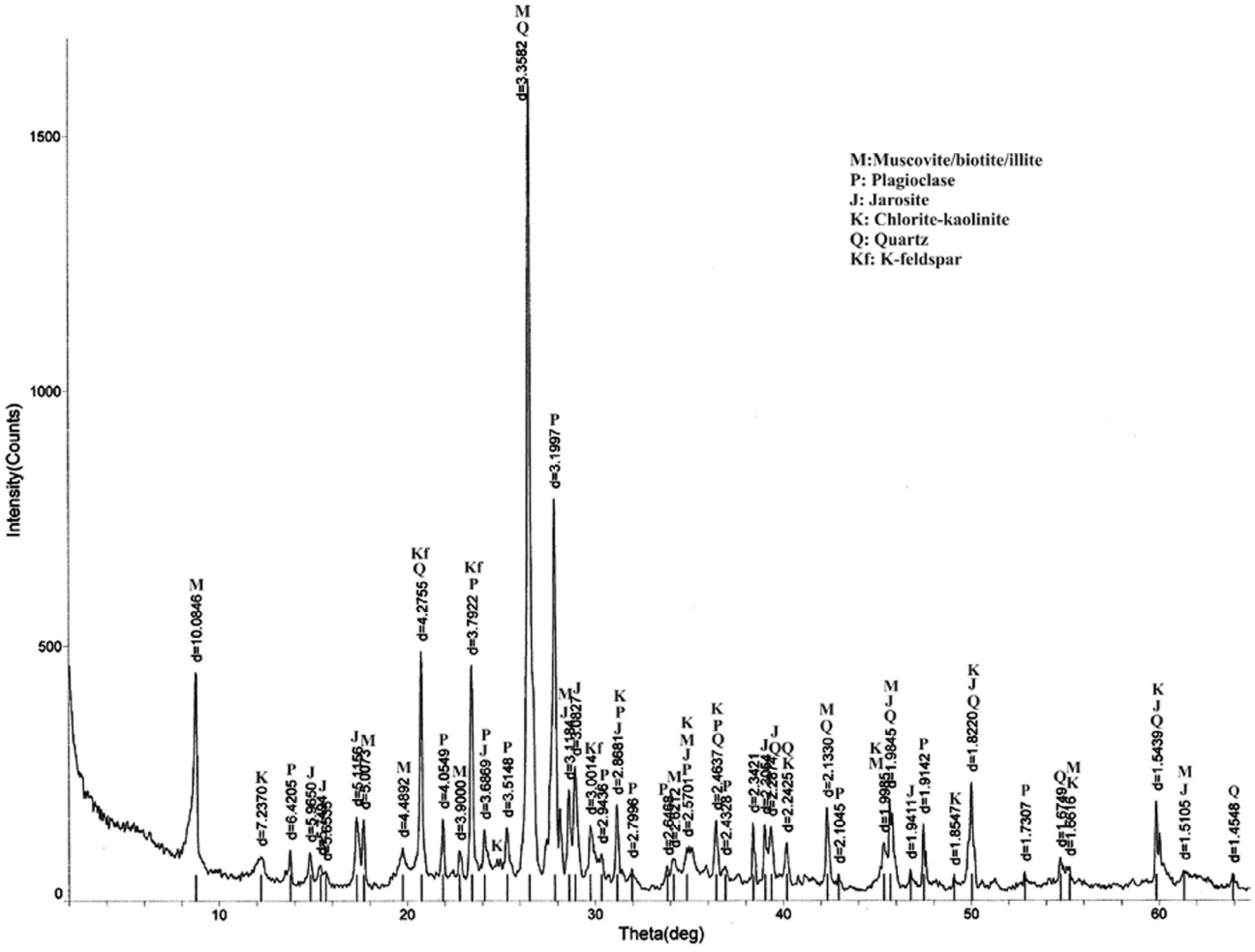


**Fig. 3.** A representative XRD pattern of sandstone host-rock.

only uranyl phosphates identified by XRD in sediments of the Koprubasi area (Fig. 4). The occurrence of autunite and torbernite is the second reported in a Koprubasi uranium deposit. In contrast to the previous brief descriptions of these minerals by Maden Tetkik Arama (1976), the identification of these minerals in the present work is based on analytical evidence including XRD and SEM-EDS.

*5.1.1. Meta-autunite (calcium uranyl phosphate)*

Meta-autunite, $Ca[(UO_2)(PO_4)]_2{\cdot}2\text{-}6H_2O$, is the most abundant uranyl mineral in the Koprubasi area. Identification of meta-autunite in Koprubasi sediments is based on XRD data and is supported by SEM/EDX spectra. It also shows brilliant greenish-yellow color under ultraviolet light. Meta-autunite occurs as damaged tabular square crystals and also in micaceous and foliated morphologies as shown in Fig. 5a. SEM and EDX spectra (marked with circle 1) showing the major elements of meta-autunite (Ca, U, P, O) with additional K (Fig. 5b). Quartz (marked with circle 2) was also observed as a dark grey phase surrounding meta-autunite.

*5.1.2. Torbernite/meta-torbernite (copper uranyl phosphate)*

The chemical formula $Cu[(UO_2)(PO_4)]_2{\cdot}8\text{-}12H_2O$ of torbernite/meta-torbernite is similar to that of autunite, but $Cu^{2+}$ replaces $Ca^{2+}$ (Locock and Burns, 2003). Identification of torbernite/meta-torbernite (lighter areas in Fig. 6a) in the Koprubasi sediments is based on XRD analysis and is supported by SEM examination. Torbernite grains can be seen in the center of Fig. 6a and are flat and square crystals (Fig. 6b). The EDX analysis (marked with circle 1) in Fig. 6b reveals primarily Cu, U, P and O with minor Mg (Fig. 6c). Meta-torbernite is a dehydration product of torbernite. Therefore, based on the SEM image in Fig. 6a (see arrows), we suggest that some torbernite decomposition to meta-torbernite has occurred.

*5.2. Associated minerals*

Uranyl phosphates coexist with jarosite, Fe and Mn-(hydr) oxides, clays and titanium oxides, but their coexistence with jarosite, Fe-(hydr) oxides and clays constitutes the most common associations in the Koprubasi sediments.

*5.2.1. Jarosite*

Jarosite is a secondary sulfate mineral. It forms under acidic, oxidizing conditions and is commonly associated with the weathering of sulfide minerals (Stoffregen et al., 2000).

Jarosite was identified in most of sediment samples of Koprubasi. Identification of jarosite is based on XRD and SEM studies (white arrows in Fig. 7a) and is substantiated by the cubic morphology (Fig. 7b) and EDX spectrum of circle 1 (in Fig. 7b) containing the major elements of jarosite (K, Fe, S and O with additional minor amounts of Si, Al and Mg). The presence of jarosite is an indicator of acidic, oxidizing environment and sulfide-bearing minerals in Koprubasi area. Jarosite has also been found in the some of outcropping gneiss by XRD analysis, was also reported by Kacmaz (2007).

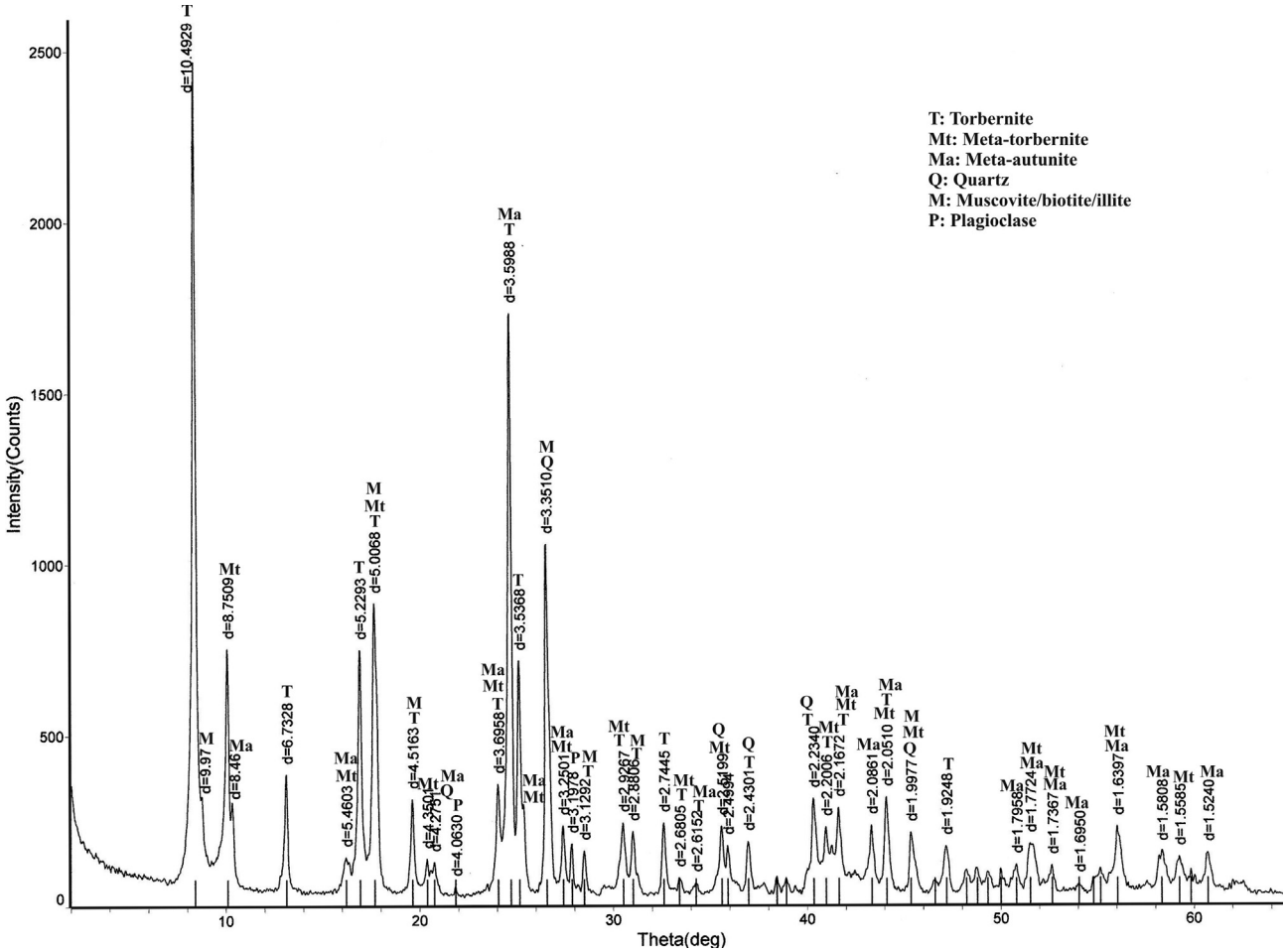


**Fig. 4.** Powder XRD pattern of sediments representing uranium mineralization for Koprubasi area.

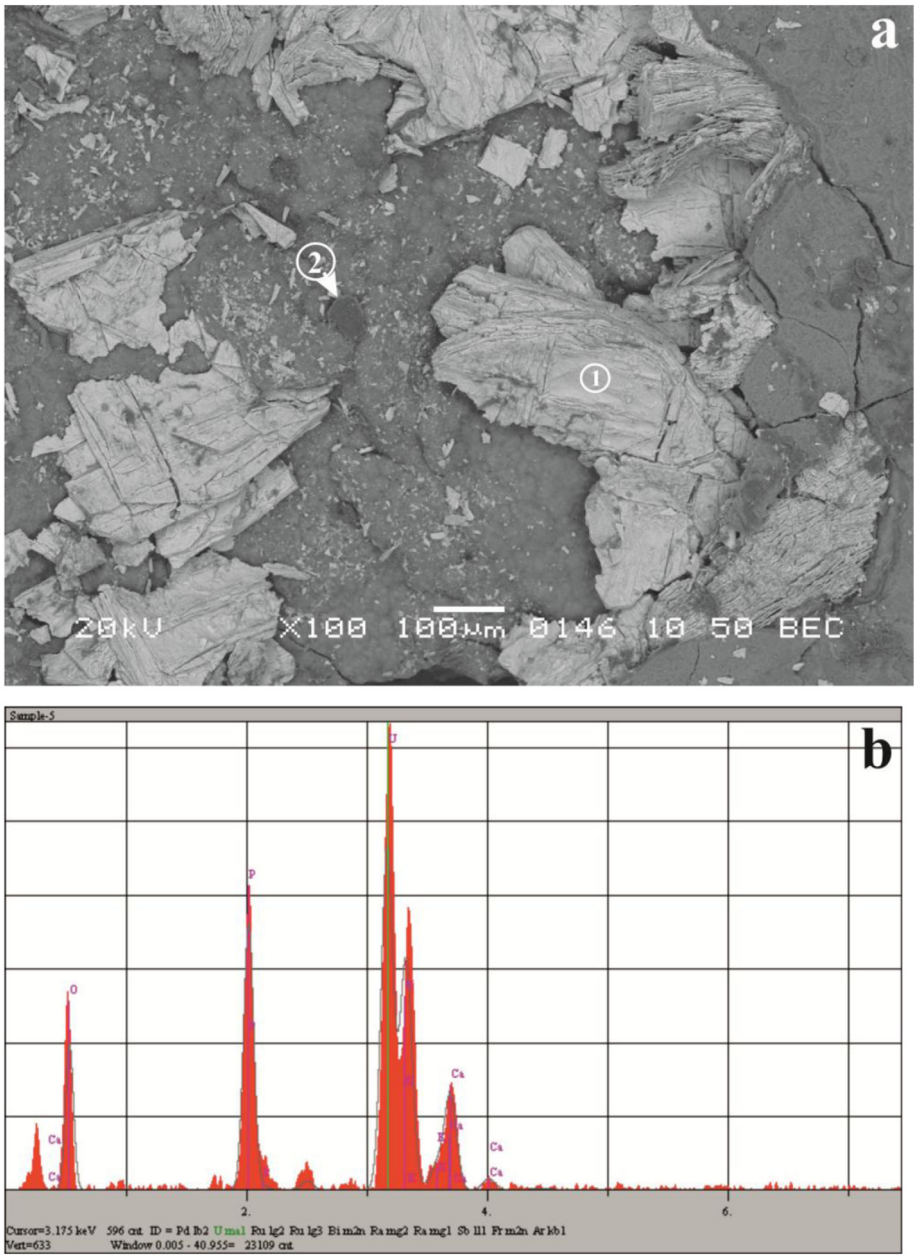


**Fig. 5.** (a) Backscattered electron image (BSE) of meta-autunite (white region), (b) EDX spectrum of the area marked with circle 1.

*5.2.2. Fe-(hydr) oxides*

In natural environments, the iron oxides exhibit different mineral phases, ranging from poorly crystalline nanophases such as 2-line ferrihydrite to coarsely crystalline phases such as goethite and hematite (Cornell and Schwertmann, 2003).

Fe-(hydr) oxides are the most common authigenic minerals in the Koprubasi sediments. The yellowish brown, reddish brown or brown-black colour of some sediment in the Koprubasi area points to the presence of iron (hydr) oxides. This suggestion is consistent with the high iron content of these sediments reported by Kacmaz (2007), some of which contain up to 18 wt.% total iron expressed as $Fe_2O_3$. However, the individual iron (hydr) oxide minerals were rarely identified by XRD in Koprubasi sediments due to the mixture of other mineral species.

SEM examinations showed that meta-autunite is commonly associated with Fe-(hydr) oxides in the Koprubasi sediments (black arrows in Fig. 8). These Fe-(hydr) oxides were identified by means of their reniform morphology (white arrows) and EDX analysis showing Fe and O as dominant elements. The prominent Si, together with minor Al, K and Ca in the EDX spectrum, may arise from the iron (hydr) oxide absorbing these elements on its surface. Although its morphology and EDX spectrum suggest that this mineral is a Fe-(hydr) oxide (probably goethite), no diagnostic XRD peaks for this mineral were observed for this sample.

However, goethite was observed with meta-autunite in the Ecinlitas area. Goethite is the only iron oxide mineral detected by XRD from Koprubasi. It was also identified by ore microscopy (G in Fig. 9a). According to Mohapatra et al. (2008), goethite having a reniform morphology represents the first-formed goethite precipitated from iron-enriched fluid at low temperature. It also contains silica and alumina. Therefore, it likely formed by the oxidation of dissolved ferrous iron in groundwater as it moved through the host rock. On the other hand, goethite, which was observed by XRD and ore microscopy in the Ecinlitas area, was not identified by SEM examination. Colloform goethite is intersected by Mn-(hydr) oxide (Fig. 9b). This indicates that goethite

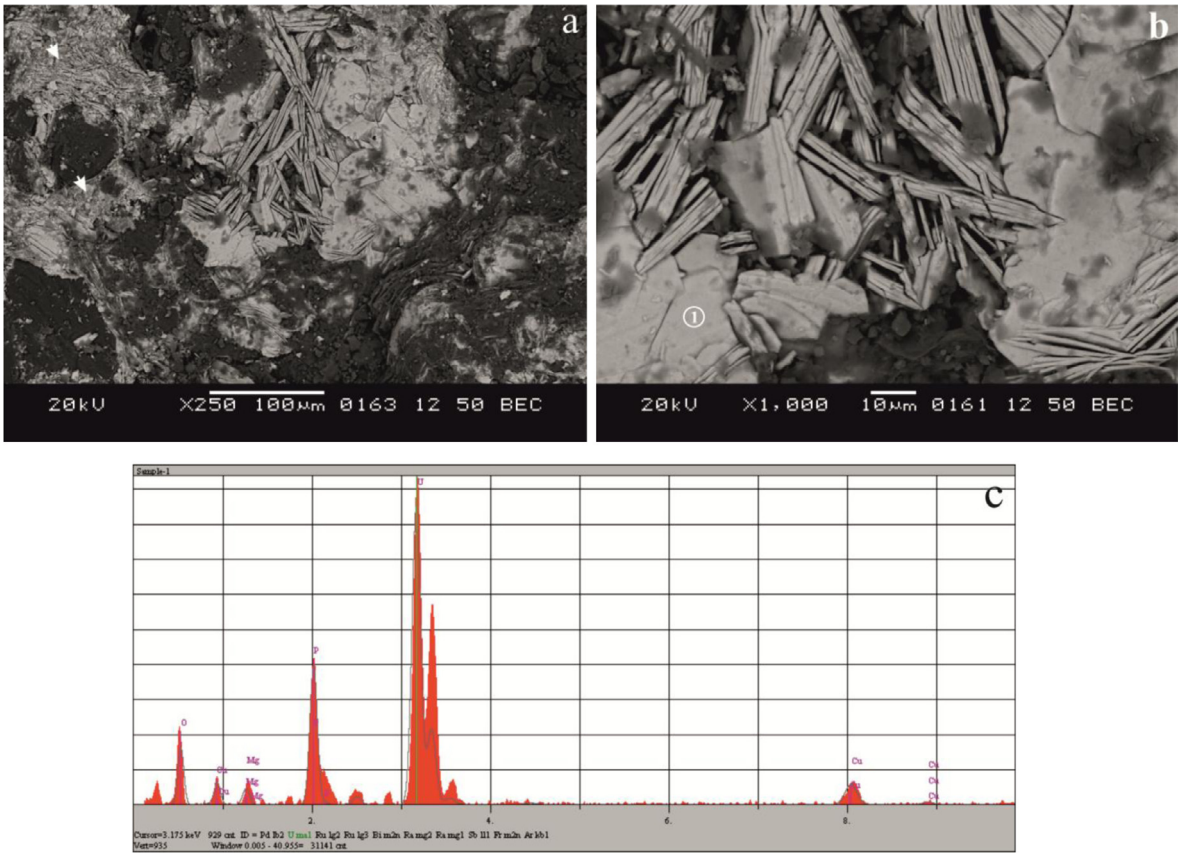


**Fig. 6.** (a) Backscattered electron (BSE) images of torbernite/meta-torbernite, (b) A close up view of the Fig. 6a center, (c) EDX spectrum of circle 1 in Fig. 6b.

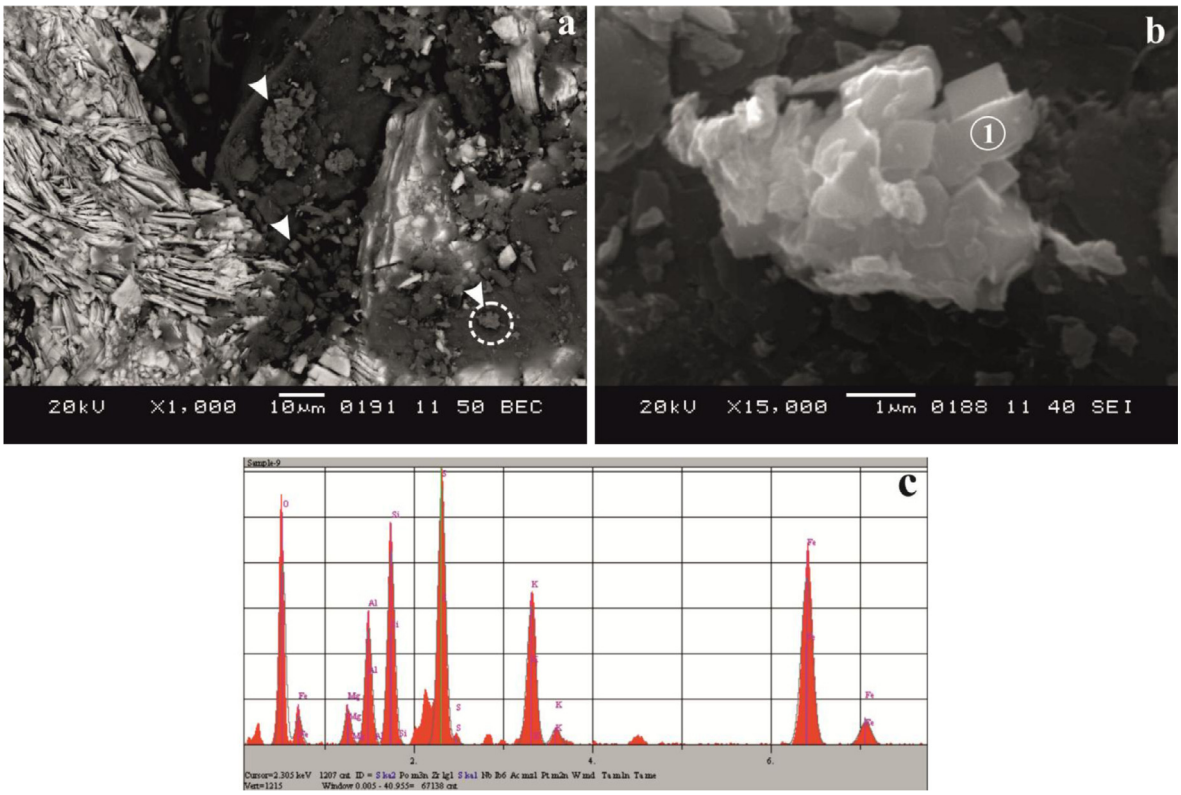


**Fig. 7.** (a) K-jarosite crystals (arrows) together with meta-autunite (lighter parts), (b) magnified view of dashed circle in Fig. 7a (c) EDX spectrum of the cubic crystal marked with circle 1.

formed before Mn-(hydr) oxide. Hence, the lack of goethite under SEM observation can be explained by Mn-(hydr) oxide coating the goethite substrate.

Additional data for goethite a surface coating of under manganese (hydr) oxide was obtained from elemental distribution maps of this sample (Fig. 10) which showed that iron (red) and manganese (orange) are enriched in same surface areas.

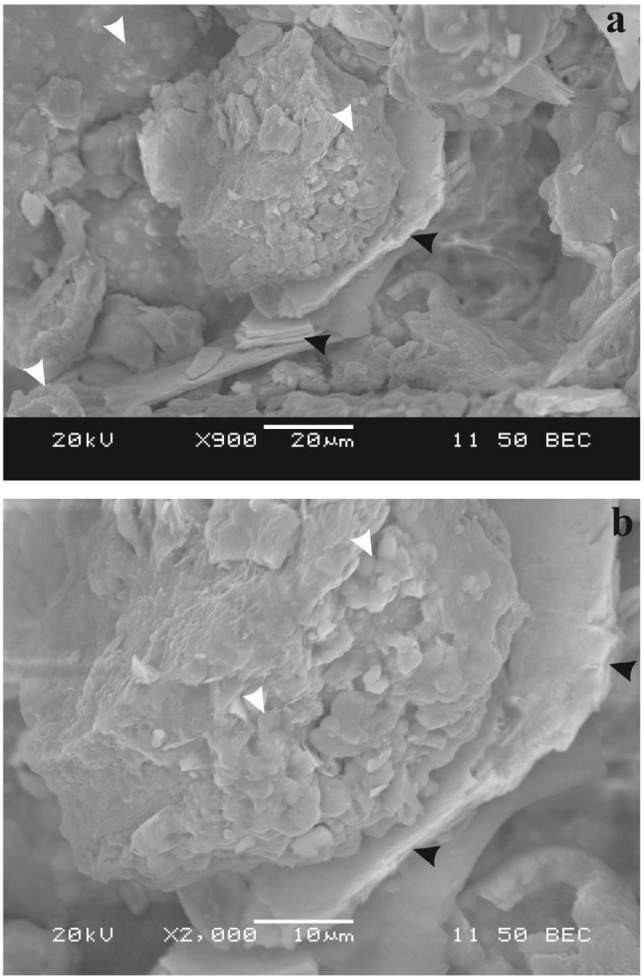


**Fig. 8.** (a) Backscattered electron (BSE) images showing the reniform iron oxyhydroxide (white arrows) associated with meta-autunite (black arrows), (b) close-up view of the iron (hydr) oxide morphology.

The presence of Fe and Mn-(hydro) oxides imply that an oxidizing environment prevailed at the time of formation of the sedimentary deposit. Dissolved forms of iron (II) and manganese (II) are generally present in high concentrations in sediments and unoxic waters. But under oxic conditions, $Fe^{2+}$ is quite rapidly oxidized. By contrast, the oxidation of $Mn^{2+}$ is relatively slower than $Fe^{2+}$ (Giblin, 2009). This probably allows for precipitation of manganese oxide on goethite surfaces as stated above.

*5.2.3. Mn-(hydr) oxide*

Mn-(hydr) oxide, which was not been detected by XRD, was observed to coexist with meta-autunite (white regions) in the Ecinlitas area of Koprubasi (Fig. 11a). Close inspection at higher magnifications (dashed square) confirms a botryoidal morphology on the surface (Fig. 11b). This crystalline habit and the EDX analysis (white circle) yielding manganese and oxygen suggest that this mineral is Mn-(hydr) oxide (maybe pyrolusite). In addition to the dominant Mn and O peaks in the EDX spectrum, the existence of minor amounts of Co, Ni, Cu, Ba, Ca, K, U, S, P, Si, and Al (Fig. 11c) is probably due to high sorption capacity of Mn oxide for these elements (Kabata Pendias, 2011; Miller et al., 2012).

The lack of diagnostic peaks of Mn-(hydr) oxides in the XRD patterns indicates that Mn-(hydr) oxides, if present, are not abundant, or are perhaps amorphous. Likewise, the manganese content of the sedimentary rocks, stated by Kacmaz (2007), is generally low to medium grade (0.01–0.1 MnO wt.%). Nevertheless, samples from the Ecinlitas area have higher MnO values up to 0.76 wt.%. Moreover, a sample from the highest Mn-containing sediment sample that also contains high iron has elevated uranium content (approximately 1 wt.%).

*5.2.4. Clays*

Uranium associated with clay minerals has been described in various geologic environments. For example, Beaufort et al. (2005) reported a close association between chloritization and uranium in the unconformity-type uranium deposit in the East Alligator rivers uranium field. Similarly, Wilson and Kyser (1987) noted uranium mineralization is associated with chlorite and illite and kaolinite in the Key Lake Uranium Deposit, Canada.

Examination of some samples under ultraviolet light revealed disseminated uranium minerals in pore spaces of the sandstones. XRD data confirm that this fluorescent mineral is meta-autunite and that it is commonly disseminated throughout a sandstone matrix containing mostly feldspar, quartz, mica, jarosite and clay minerals. XRD patterns of these sandstones usually show reflection at ca. 10 and 7.2 Å, corresponding to muscovite/illite/biotite and chlorite/kaolinite, respectively. Some samples from the mudstone

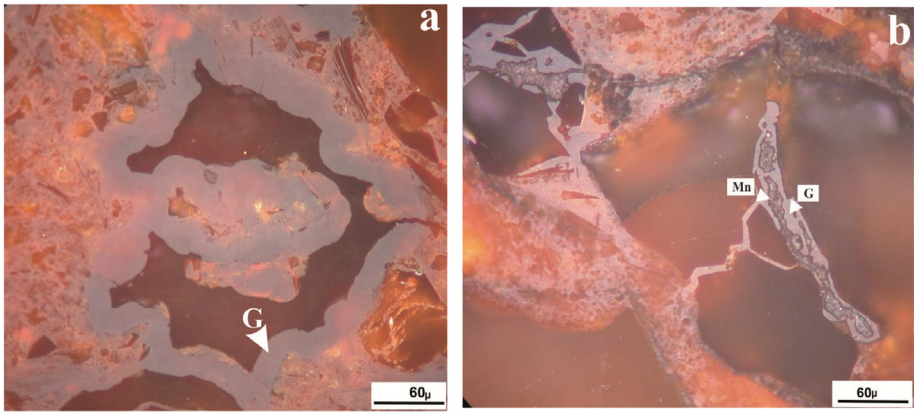


**Fig. 9.** (a) Goethite (G) in colloform texture, (b) Mn-(hydr) oxides (Mn) with early-formed colloform goethite (reflected light of polished section).

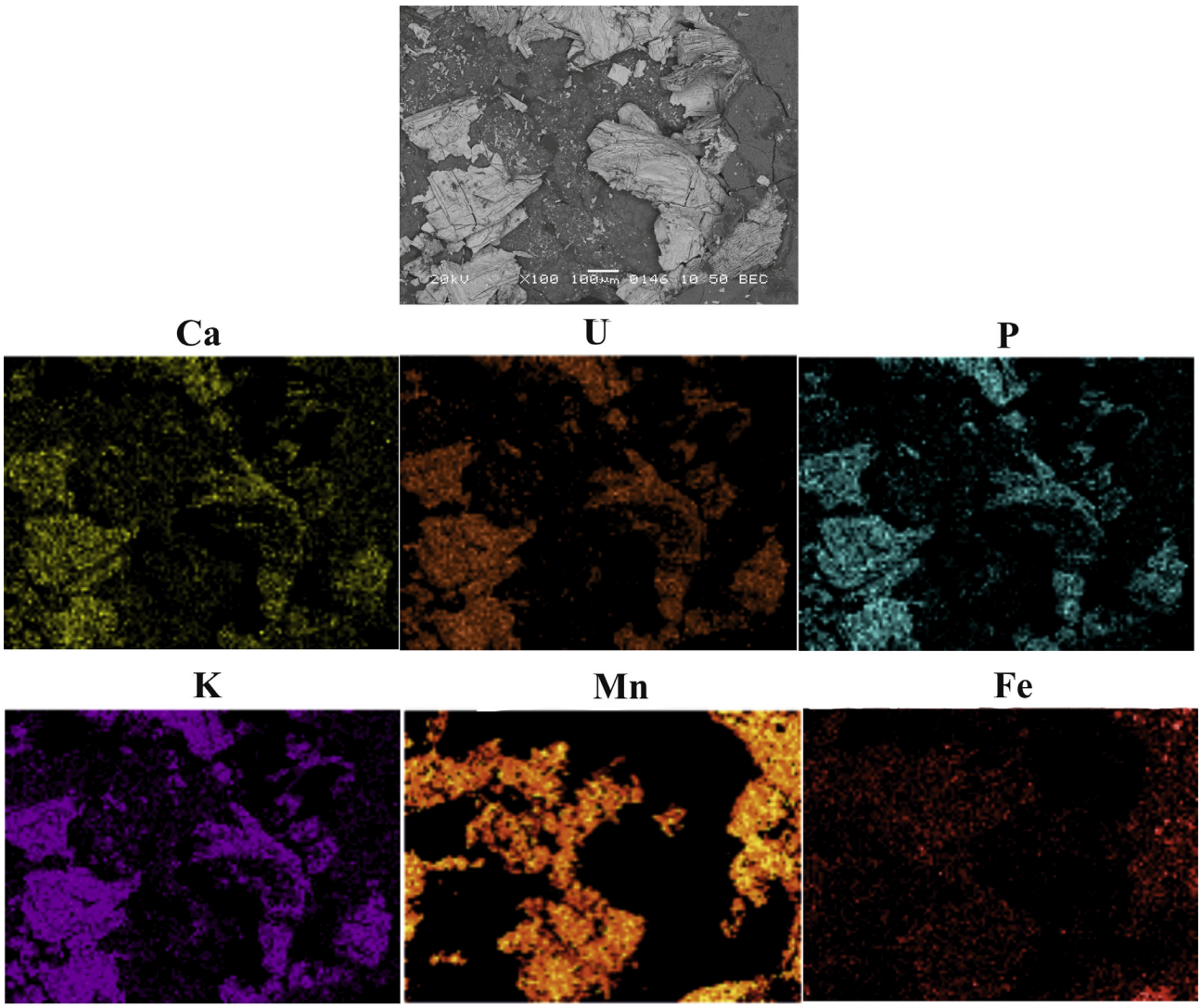


**Fig. 10.** X-ray elemental map of the selected sample shows the elemental distribution of Ca, U, P, K, Mn, and Fe in selected BSE image. Fig. 10 also confirms goethite with manganese (hydr) oxide in this sample.

and conglomerate display a broad diffraction peak in the vicinity of 15 Å due to either smectite or chlorite.

SEM observations of sandstone reveal that meta-autunite is disseminated at the micron scale (bright areas in Fig. 12a), occurring parallel to the cleavage planes of partially degraded biotite as shown in Fig. 12b. Identification of biotite (probably chloritized biotite) is based on its morphology and EDX spectrum containing the major elements of biotite (Si, Al, Mg, K and Fe). Likewise, the conversion of biotite to chlorite observed here is also clearly seen by polarizing microscopy in investigated samples (Kacmaz, 2007). Similar uranium enrichment in the partially weathered biotite was reported by Ryan and O' Beirne-Ryan (2006) in arkosic sandstone of the Horton Group near Windsor, Nova Scotia, Canada.

Microcrystalline meta-autunite was observed within the clay-rich sandstone matrix (brightest grain about 10 µm width in Fig. 13a). EDX spectra corresponding to the white circles in Fig. 13a show that the matrix where Si, Al, Fe, K and Mg exist (Fig. 13b) contains a high percentage of iron oxide. Therefore, based on the EDX data, we can suggest that these minerals are iron-rich clays (possibly chlorite). The white arrows in Fig. 13a indicate pseudo-cubic crystals of jarosite.

Moreover, illite flakes were observed as a grey phase surrounding meta-autunite (white region in Fig. 14a) within mudstone. Identification of illite is based on its morphology (Fig. 14b) and the EDX spectrum (Fig. 14c) showing the major elements of illite (Si, Al and K with a minor amount of Fe). Semi-quantitative spectra obtained from white crystals (in Fig. 14a) clearly indicate Ca, U and P (meta-autunite) with trace amount of Al and Si.

Kaolinite was also observed to coexist with meta-autunite (white region in Fig. 15a) in the same sample. Identification of the kaolinite is based on its morphology (Fig. 15b) and EDX analysis (Fig. 15c) which shows the major elements of kaolinite (Si, Al, Fe and organic C with minor amounts of K, Ca and Na). Its high iron content could be explained by some of the Al cations substituted by Fe ions as stated by Bauluz et al. (2008) for kaolinite from Albanian sedimentary deposit of the Southern Iberian Range (Spain). Minor amounts of K, Ca, and Na, perhaps due to interference by illite or smectite, were seen in this sample.

Kaolinite and illite in the matrix of the mudstone are probably due to weathering of either micas (biotite, muscovite) or K-feldspar in the Koprubasi area.

*5.2.5. Titanium oxides*

Titanium oxides present another association with uranium in the Koprubasi sediments. Their coexistence with uranyl phos-

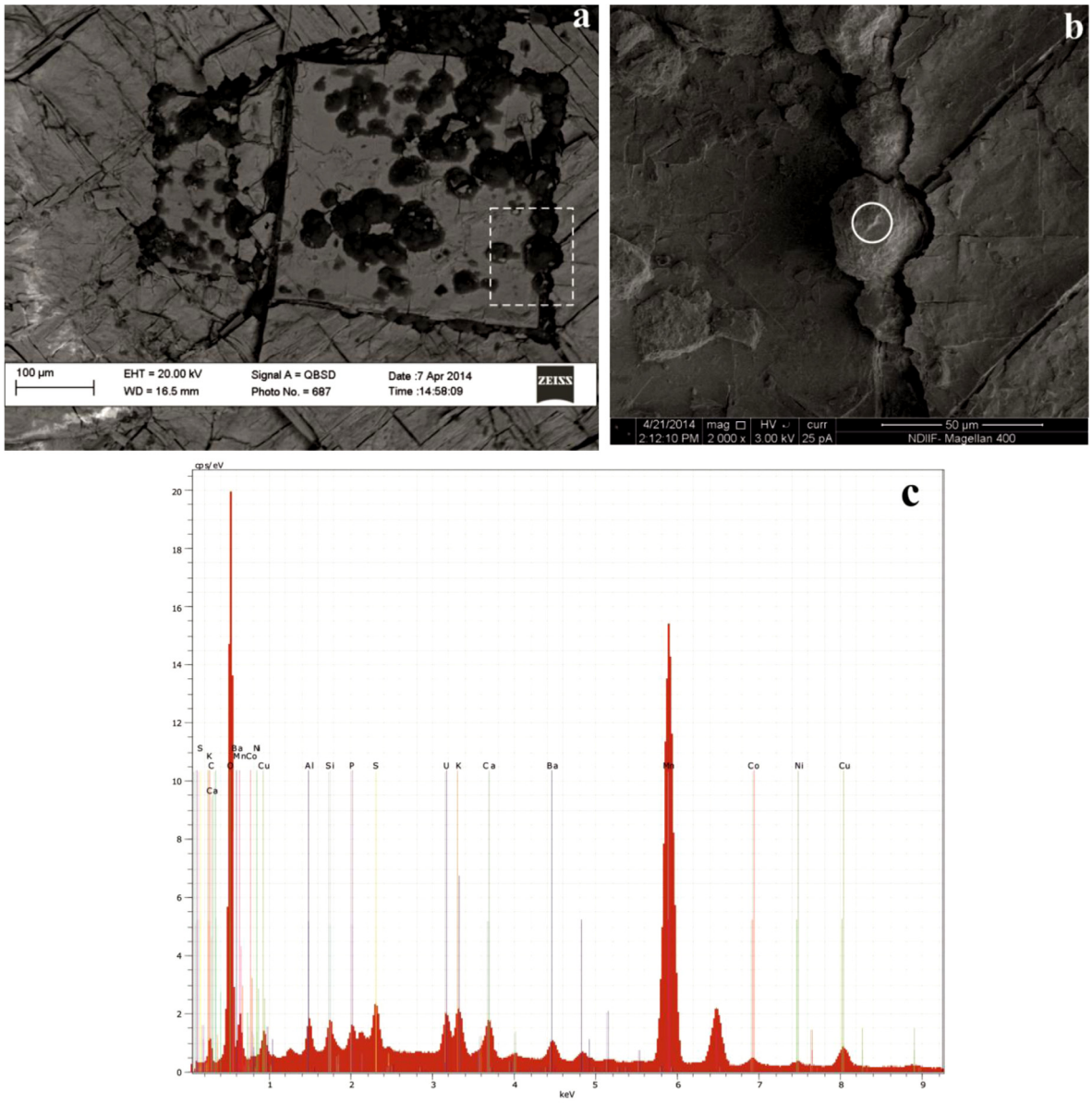


**Fig. 11.** (a) Backscattered electron (BSE) images showing meta-autunite (light areas) with Mn-(hydr) oxides (dark areas), (b) Magnified view of dashed square showing characteristic botryoidal morphology, (c) EDX spectrum showing the composition of the bubble (white circle).

phates was observed in mudstones comprised of a clay-rich matrix (kaolinite and illite).

SEM examination of samples shows that small titanium oxide grains are concentrated on and around meta-autunite crystals (white region in Fig. 16a) in the clay rich matrix. The grains have diameters less than 1 µm, making it difficult to isolate them using EDX analysis. However, the EDX spectrum of multiple grains (dashed circle in Fig. 16b) reveals Ti as the major element with trace amounts of Fe, Ca, Si, Al and K (Fig. 16c) that are probably signals from underlying minerals. The surface of the meta-autunite is coated with titanium oxide grains (all small grains in Fig. 16b). The appearance of titanium oxides on meta-autunite indicates that titanium oxides formed later than meta-autunite. Here, titanium oxide grains (uncertain composition) probably occurred due to intense weathering of titanium-containing minerals (either of rutile, ilmenite or micas) in the host rock. Jarosite peaks were not detected by XRD for this sample, although its crystalline habit and the EDX spectrum suggest that cubic minerals are jarosite (white arrows in Fig. 16a).

### *5.3. Effect of Fe-(hydr) oxides and clays on the precipitation of uranyl phosphates*

Uranium is present in oxidizing groundwater as the uranyl species ($UO_2^{2+}$), which tends to be an uncomplexed form at low pH values (Vandenhove et al., 2010). At higher pH, the U(VI) ion forms very stable complexes with some of the major constituents dissolved in natural water such as carbonate, sulfate and phosphate. If the activity of the dissolved complex is high, uranyl minerals can directly precipitate from groundwater (Finch and Murakami, 1999).

The uranyl ion can be adsorbed from solution by iron hydroxides and clays (Kovačević et al., 2009; Haglund, 1972; Ames et al., 1982; Duff et al., 2002) and this is an important mechanism for precipitation of uranium in natural environment. The two most important factors influencing the adsorption of U(VI) are pH and dissolved carbonate concentration (Muto et al., 1965; USEPA, 1999). According to Dall'aglio et al. (1974) the reaching of high U (VI) activity in circulating water due to low concentration of the

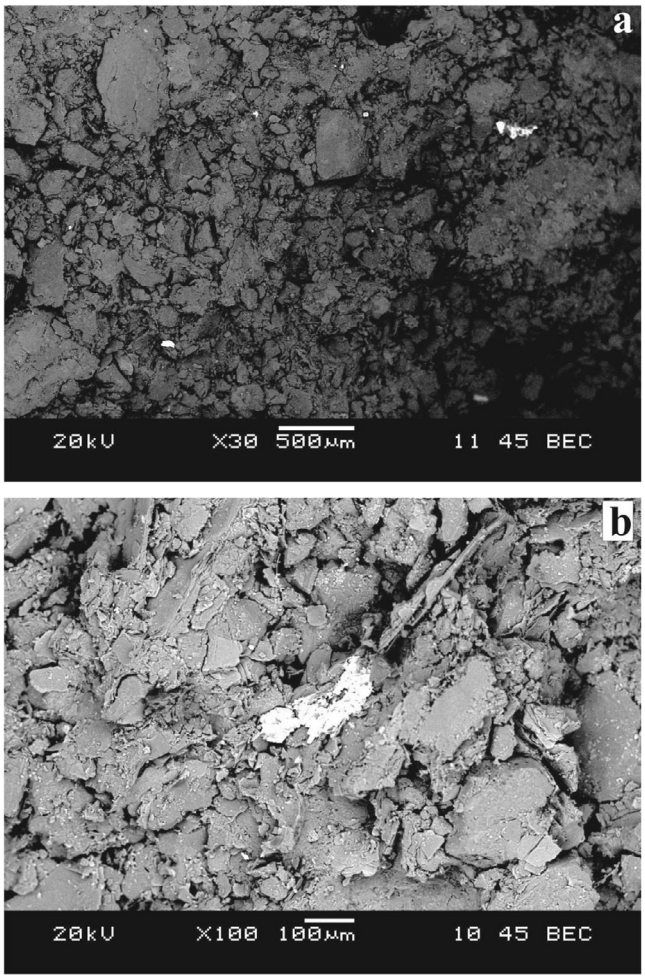


**Fig. 12.** (a) Disseminated meta-autunite microcrystals (bright areas) in sandstone, (b) Enlarged view of one of bright areas in Fig. 12a indicating that disseminated meta-autunite occurs in partially degraded biotite boundary.

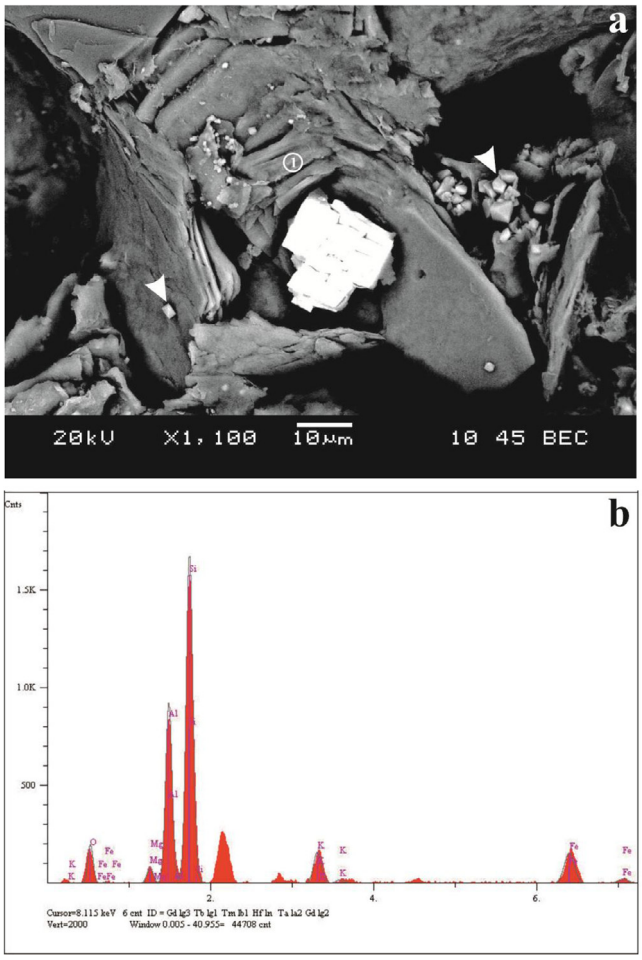


**Fig. 13.** (a) Backscattered electron image of meta-autunite (brightest grain) associated with jarosite (pseudo-cubic crystals) within iron-rich clays, (b) EDX pattern of the area marked with circle 1.

carbonate ion which is an effective uranyl complexing ligand. Because, carbonate ions form highly stable solution complexes with the uranyl ion and this causes a lowering of the activity of uranyl ion (Yeh and Tripathi, 1991; Duff and Amrhein, 1996). Therefore, uranium sorption to iron oxides and clays is extensive in the absence of dissolved carbonate, as demonstrated experimentally by Ames et al. (1982). In addition, U(VI) adsorption to iron oxides typically increases from low to near neutral pH conditions (Langmuir, 1997).

On the other hand, dissolved phosphate is a common constituent of many groundwaters (Finch and Murakami, 1999) and it is also an important ligand that affects U(VI) adsorption. Experimental studies by Cheng et al. (2004) and Bachmaf et al. (2008) indicate that phosphates can enhance U(VI) adsorption onto clays and Fe (III) oxides (like goethite) by the formation of ternary surface complexes. The work of Munasinghe et al. (2009) showed that the precipitation of autunite-group minerals occurs rapidly in the presence of goethite and mica. Murakami et al. (1997) showed the formation of saléeite (magnesium uranyl phosphate) microcrystals on the surface of goethite as a result of local saturation although bulk groundwater was undersaturated with respect to this mineral. Recent work by Schindler and Ilton (2013) suggests that interaction of U-bearing solutions with Fe-hydroxides containing adsorbed phosphate in aquifer can result in the precipitation of autunite group minerals.

Chemical evaluation of present-day groundwater samples from the oxidizing host rock aquifer of Koprubasi area (Kacmaz and Nakoman, 2009) revealed that these groundwater are undersaturated with respect to torbernite, autunite and calcite while they are saturated or supersaturated with respect to hematite, goethite, muscovite, illite, kaolinite and quartz. In addition, these oxic groundwaters have low carbonate alkalinity.

Kacmaz and Nakoman (2009) also showed that dissolved Fe concentration in these groundwater are positively correlated with both dissolved U(VI) and phosphate concentrations (Fe:U = 0.94 and Fe:$PO_4^{3-}$ = 0.94 respectively).

A minor amount of macroscopic uranyl phosphates was seen with the naked eye within small gaps of some sediments. In addition, the widespread appearance of macroscopic and microscopic uranyl phosphates with Fe-(hydr)oxides (like goethite) and within clay rich matrices indicate their surface precipitation with both Fe-(hydr)oxides and clays. Similar mechanisms for uranium phosphate formation have been described by Schindler and Ilton (2013), Schindler et al. (2015), Singh et al. (2010), Singh (2010), Sato et al. (1997) and Jerden and Sinha (2006).

From the observed data, we suggest that the dominant mechanism for formation of uranyl phosphate minerals in Koprubasi sediments is adsorption of uranyl and phosphate onto Fe (hydr) oxides and clays, followed by recrystallization. Hence, the precipitation of uranyl phosphates, torbernite, meta-torbernite and meta-autunite, has mostly occurred along with iron (hydr) oxides

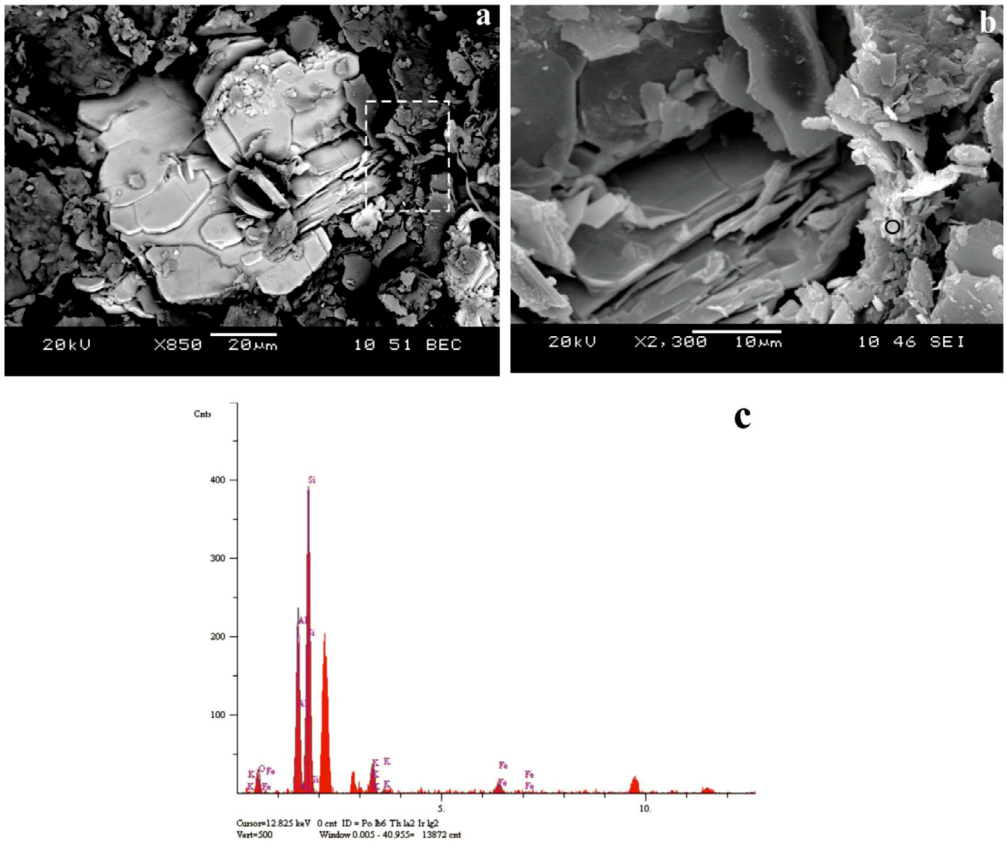


**Fig. 14.** (a) Backscattered electron image of meta-autunite (white region) and the area around it, (b) Close-up view of dashed rectangle in Fig. 14a, (c) EDX spectrum of area marked with black circle in Fig. 14b.

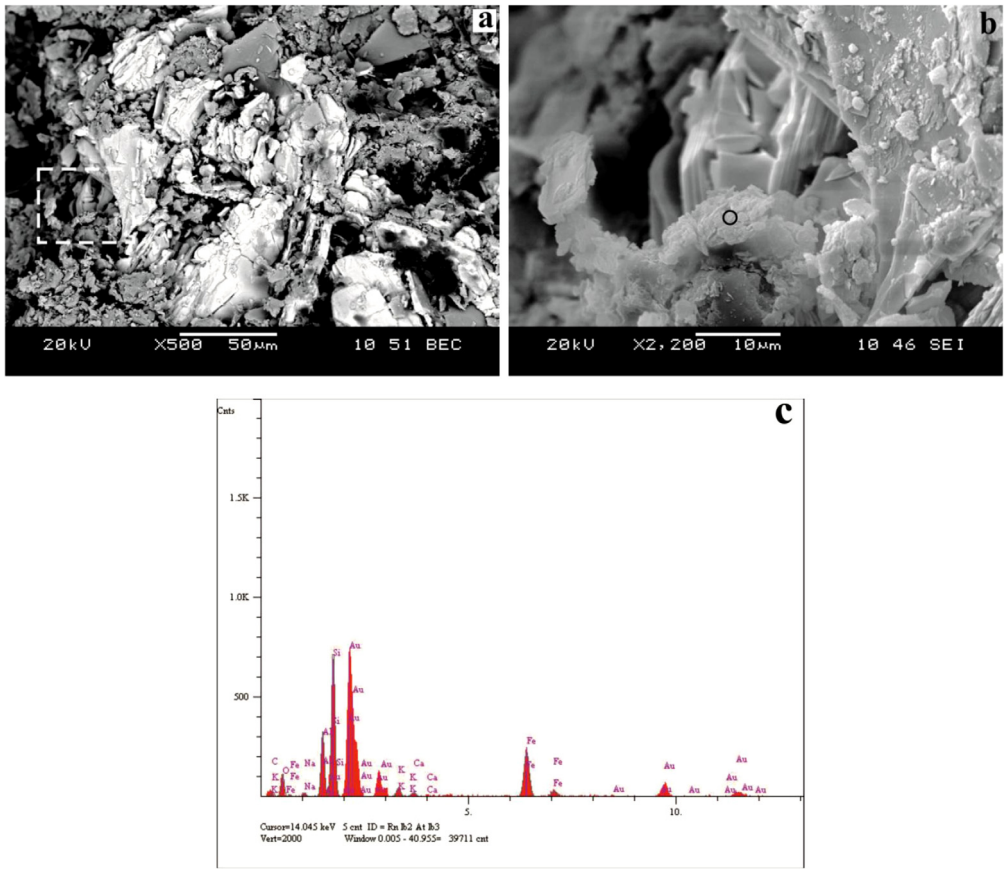


**Fig. 15.** (a) BSE image of meta-autunite (white region) in a clay-rich mudstone matrix, (b) An enlarged view of the dashed rectangular area in Fig. 15a (c) EDX spectrum of the area marked black circle in Fig. 15b.

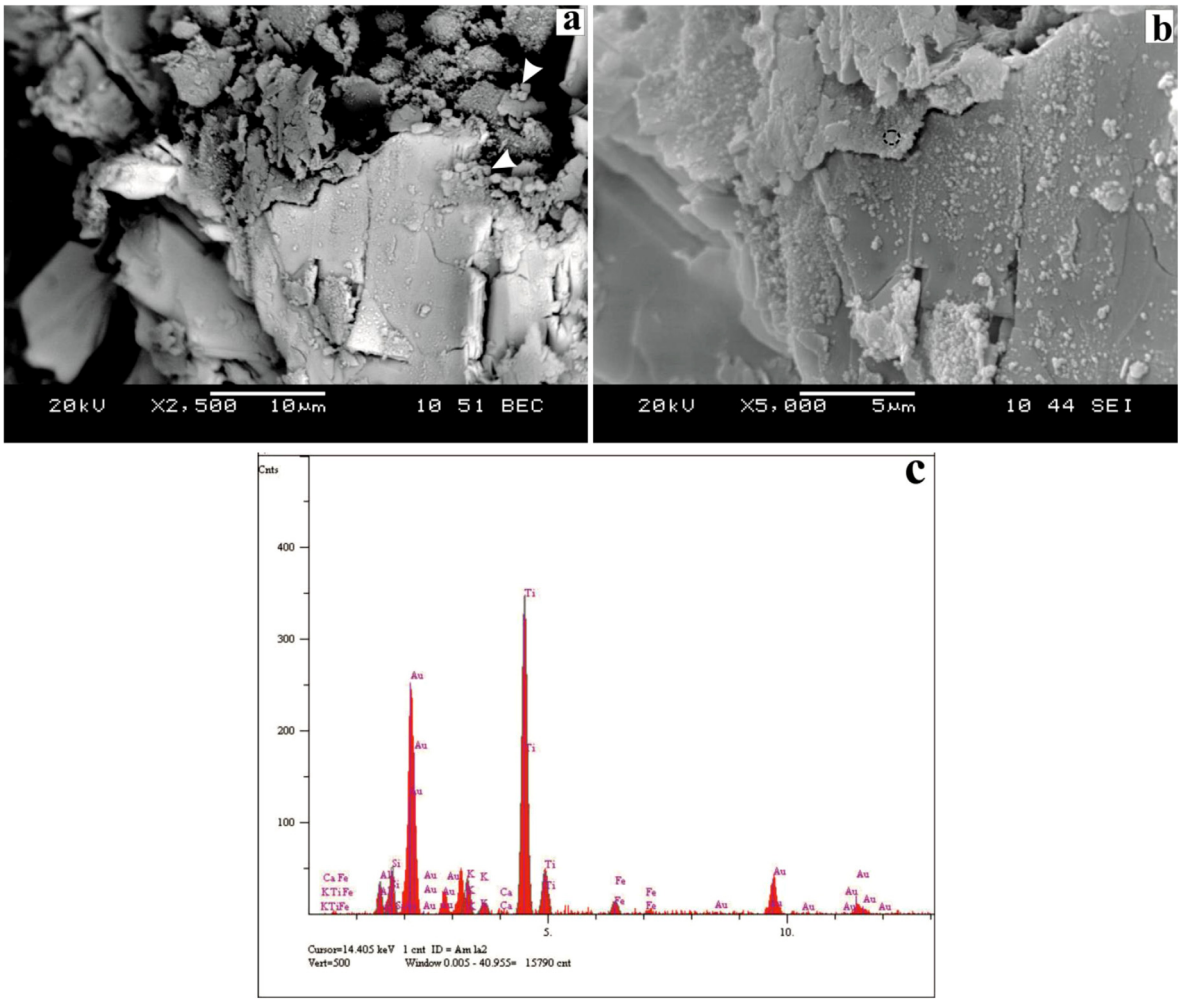


**Fig. 16.** (a) BSE image of titanium oxide grains on and around meta-autunite in the clay rich matrix of mudstone, (b) An enlarged SEM view of Fig. 16a center, (c) The EDX spectrum of dashed circle in Fig. 16b.

and clays. It is also possible that low carbonate alkalinity of groundwater in the oxidizing host rock aquifer facilitated the adsorption of U(VI) to the Fe-(hydr) oxides and clays. Significant positive correlation of dissolved Fe with U and phosphate might be an indicator of Fe-(hydr) oxides influencing adsorption of U and P from groundwater.

## 6. Conclusion

We characterized uranyl phosphates and associated minerals, and evaluated their paragenetic relationships. The minerals identified by XRD in sediments are primarily meta-autunite, torbernite, meta-torbernite, quartz, feldspars, mica (muscovite/biotite), jarosite and clays (illite, chlorite/kaolinite, smectite), with a lesser amount of goethite. Mn-(hydr) oxides and titanium oxides were not detected by XRD, but were observed either by optical or SEM.

The uranium mineralization is mainly associated with Fe-(hydr) oxides and clays, although minor Mn-(hydr) oxides also occur with uranyl phosphates.

The uranyl phosphates were likely formed due to movement of uranium-bearing oxidizing groundwater into the host sedimentary rock. Fe-(hydr) oxides and clays are the most important minerals affecting the precipitation of uranyl phosphates in Koprubasi area.

## Acknowledgement

This study has been supported by Tubitak (Bideb 2219) post-doctoral fellowship for research abroad at the University of Notre Dame, Indiana, USA. The authors thank Dr. R. Finch and an anonymous referee for their constructive comments and recommendations.

## References

Ames, L.L., McGarrah, J.E., Walker, B.A., Salter, P.F., 1982. Sorption of uranium and cesium by Hanford basalts and associated secondary smectites. Chem. Geol. 35, 205–225.

Bachmaf, S., Planer-Friedrich, B., Merkel, J.M., 2008. Effect of sulphate, carbonate, and phosphate on the uranium (VI) sorption onto bentonite. Radiochim. Acta 96, 359–366.

Bauluz, B., Mayayo, M.J., Yuste, A., Gonzalez Lopez, J.M., 2008. Genesis of kaolinite from Albian sedimentary deposits of the Iberian Range (NE Spain): analysis by XRD, SEM and TEM. Clay Miner. 43, 459–475.

Beaufort, D., Patrier, P., Laverret, E., Bruneton, P., Mondy, J., 2005. Clay alteration associated with Proterozoic unconformity-type uranium deposits in the East Alligator River uranium field, Northern Territory, Australia. Econ. Geol. 100, 515–536.

Cheng, T., Barnett, M.O., Roden, E.E., Zhuang, J.L., 2004. Effects of phosphate on Uranium (VI) adsorption to goethite-coated sand. Environ. Sci. Technol. 38 (22), 6059–6065.

Cornell, R.M., Schwertmann, U., 2003. The Iron Oxides: Structure, Properties, Reactions, Occurrence and Uses. Wiley-VCH.

Dall'aglio, M., Gragnani, N., Locardi, E., 1974. Geochemical factors controlling the formation of the secondary minerals of uranium. Formation of Uranium Ore Deposits. International Atomic Energy Agency, Vienna, pp. 33–48.
Duff, M.C., Coughlin, J.U., Hunter, D.B., 2002. Uranium coprecipitation with iron oxide minerals. Geochim. Cosmochim. Acta 66 (20), 3533–3547.
Duff, M.C., Amrhein, C., 1996. Uranium (VI) adsorption on goethite and soil in carbonate solution. Soil Sci. Soc. Am. J. 60, 1393–1400.
Finch, R., Murakami, T., 1999. Systematics and paragenesis of uranium minerals. In: Burns, P.C., Finch, R. (Eds.), Uranium: Mineralogy, Geochemistry and the Environment, vol. 38. Mineralogical Society of America, Washington DC, pp. 91–180.
Giblin, A.E., 2009. Iron and manganese. In: Likens, G.E. (Ed.), Biogeochemistry of Inland Waters. Elsevier Inc., pp. 368–377.
Haglund, D.S., 1972. Uranium: element and geochemistry. In: Fairbridge, R.S. (Ed.), The Encyclopedia of Geochemistry and Environmental Sciences. Dowden, Hutchicson and Ross Inc., Stroudsburg, Pennsylvania, pp. 1215–1222.
Jerden, J.L., Sinha, A.K., 2006. Geochemical coupling of uranium and phosphorous in soils overlying an unmined uranium deposit: Coles Hill, Virginia. J. Geochem. Explor. 91, 56–70.
Kabata Pendias, A., 2011. Trace elements in soils and plants. CRC Press/Taylor & Francis Group, Boca Raton, London, New York.
Kacmaz, H., 2007. Manisa-Salihli-Köprübaşı Uranyum zuhurunun incelenmesi PhD. Dokuz Eylül Universitesi, Fen Bilimleri Enstitüsü, Izmir [in Turkish].
Kacmaz, H., Nakoman, M.E., 2009. Hydrochemical characteristics of shallow groundwater in aquifer containing uranyl phosphate minerals, in the Koprubasi (Manisa) area, Turkey. Environ. Earth Sci. 59, 449–457.
Kovačević, J., Nikić, Z., Papić, P., 2009. Genetic model of uranium mineralization in the Permo-Triassic sedimentary rocks of the Stara Planina eastern Serbia. Sed. Geol. 219, 252–261.
Langmuir, D., 1997. Aqueous Environmental Geochemistry. Prentice Hall, Upper Saddle River, New Jersey.
Locock, A.J., Burns, P.C., 2003. Crystal structures and synthesis of the copper-dominant members of the autunite and meta-autunite groups: tobernite, zeunerite, metatorbernite and metazeunerite. Can. Mineral. 41, 489–502.
Maden Tetkik Arama (1976) Köprübaşı Bölgesi Uranyum yataklarına ait rapor, MTA Enstitüsü, Radyoaktif Mineraller ve Kömür Dairesi Başkanlığı, Radyoaktif Mineraller Arama Servisi, Ankara [in Turkish].
Miller, A.Z., Dionísio, A., Sequeira Braga, M.A., Hernández-Mariné, M., Afonso, M.J., Muralha, V.S.F., Herrera, L.K., Raabe, J., Fernandez-Cortes, A., Cuezva, S., Hermosin, B., Sanchez-Moral, S., Chaminé, H., Saiz-Jimenez, C., 2012. Biogenic Mn oxide minerals coating in a subsurface granite environment. Chem. Geol. 322–323, 181–191.
Mohapatra, B.K., Jena, S., Mahanta, K., Mishra, P., 2008. Goethite morphology and composition in banded iron formation, Orissa, India. Resour. Geol. 58 (3), 325–332.
Munasinghe, P., Kendall, M.R., Elwood Madden, M.E., Madden, A.S. (2009). Precipitation of uranyl phosphate influenced by mineral surfaces, GSA Annual Meeting, Paper No. 168-5.
Murakami, T., Ohnuki, T., Isobe, H., Sato, T., 1997. Mobility of uranium during weathering. Am. Mineral. 82, 888–899.
Muto, T., Hirono, S., Kurata, H., 1965. Some aspects of fixation of uranium from natural waters. Min. Geol. 15 (74), 287–298.
Ryan R.J., O' Beirne-Ryan., A.M., 2006. Preliminary Report on the Origin of Uranium Occurrences in the Horton Group of the Windsor Area, Nova Scotia Department of Natural Resources, Report of Activities, pp. 137–157.
Sato, T., Murakami, T., Yanase, N., Isobe, H., Payne, T.E., Airey, P.L., 1997. Iron nodules scavenging uranium from groundwater. Environ. Sci. Technol. 31, 2854–2858.
Schindler, M., Ilton, E.S., 2013. Uranium mineralogy and geochemistry on the nano- to micrometre scale: Redox, dissolution and precipitation processes at the mineral-water interface. In: Uranium- Cradle to Grave, P.C. Burns, G. Sigmon (Eds.), Min. Assoc. Can. Short Course 43, 203–253.
Schindler, M., Legrand, C.A., Hochella, M.F., 2015. Alteration, adsorption and nucleation processes on clay-water interfaces: Mechanisms for the retention of uranium by altered clay surface on the nanometer scale. Geochim. Cosmochim. Acta 153, 15–36.
Singh, A., 2010. Geochemical conditions affecting uranium (VI) fate and transport in soil and groundwater in the presence of phosphate, Electronic Theses and Dissertations, Washington University in St Louis, Missouri.
Singh, A., Ulrich, K.U., Giammar, D.E., 2010. Impact of phosphate on U(VI) immobilization in the presence of goethite. Geochim. Cosmochim. Acta 74, 6324–6343.
Stoffregen, R.E., Alpers, C.N., Jambor, J.L., 2000. Alunite-Jarosite crystallography, thermodynamics, and geochemistry. In: Alpers, C.N., Jambor, J.L., Nordstrom, D. K. (Eds.), Sulfate Minerals: Crystallography, Geochemistry and Environmental Significance, vol. 40. Mineralogical Society of America, Washington, D.C., pp. 453–479. and Geochemical Society, Reviews in Mineralogy and Geochemistry.
USEPA, 1999. Understanding Variation in Partition Coefficient, Kd, Values. Volume II: Review of Geochemistry and Available Kd Values for Cadmium, Cesium, Chromium, Lead, Plutonium, Radon, Strontium, Thorium, Tritium (3H), and Uranium, Office of Air and Radiation, EPA/402-R-99-004B, August.
Vandenhove, H., Hurtgen, C., Payne, T.E., 2010. Uranium. In: Atwood, D.A. (Ed.), Radionuclides in the Environment. John Wiley & Sons, Ltd, United Kingdom, pp. 261–272.
Wilson, M.R., Kyser, K., 1987. Stable isotopes geochemistry of alteration associated with the Key Lake uranium deposit, Canada. Econ. Geol. 82, 1540–1557.
Yeh, G.T., Tripathi, V.S., 1991. A model for simulating transport of reactive multispecies components: model development and demonstration. Water Resour. Res. 27, 3075–3094.
Yılmaz, H., 1982. Neojen çökelleri (Köprübaşı–Gördes) içindeki uranyum yataklarının oluşumu. JMO 5, 3–19 [in Turkish].